A Study on Nanofiller Effects of Serpentine in Polypropylene Matrix

Semra Tan, Teoman Tinçer

Department of Chemistry, Middle East Technical University, TR-06531 Ankara, Turkey

Received 14 January 2011; accepted 14 June 2011
DOI 10.1002/app.35162
Published online 18 October 2011 in Wiley Online Library (wileyonlinelibrary.com).

ABSTRACT: The nanocomposite materials were prepared using serpentine as filler and polypropylene (PP) as the matrix in the presence of maleic anhydride grafted polypropylene (PP-*g*-MA) compatibilizer. The melt intercalation was carried out following serpentine modification with a quaternary salt of cetyl-trimethyl-ammonium bromide. The structure of nanocomposites was shown by X-ray diffraction (XRD) and transmission electron microscopy (TEM) studies. Thermal analysis performed by differential scanning calorimetry (DSC) demonstrated that the nanocomposites have higher percentage crystallinity when compared to neat PP. Dynamic mechanical analysis (DMA) revealed that the storage and loss moduli values of the nanocomposites are better than those of the matrix resin. Tensile properties of nanocomposites are significantly different from PP, e.g., the Young's modulus of the nanocomposite with 2 wt % serpentine and 6 wt % PP-*g*-MA (PP-2,6Q) was found to be 2065 MPa, i.e., nearly 190.8% increase over the PP matrix. © 2011 Wiley Periodicals, Inc. J Appl Polym Sci 124: 1419–1425, 2012

Key words: PP nanocomposites; serpentine; DMA; mechanical properties

INTRODUCTION

Polymer clay nanocomposites comprise an important subclass of polymer nanocomposites, gaining increasing interest both scientifically and industrially. They show excellent improvements in strength, modulus, scratch and solvent resistance, barrier, thermal and flammability properties, ionic conductivity, and heat distortion temperature.[1,2] Montmorillonites have received a lot of attention as layered silicate fillers due to their availability and ease of surface modification. These clay minerals have one dimension in nanometer range, i.e., while the sheets can extend to thousands of nanometers thicknesses vary in the subnanometer range.[3–5] Generally, clays are treated by quaternary ammonium salts so as to improve their adhesion with matrix, through which the exchange of cations is possible. The exchange reactions are also advantageous in that the basal spacing between the layers of clay increases due to the presence of bulky organic ions. The alkyl ammonium and alkyl phosphonium cations reduce the surface energy of the clay and improve the wetting characteristics with the polymer.[6,7]

The work done by Toyota research group on nylon 6-montmorillonite pioneered the use of clays in polymer matrices. It was observed that the silicate layers of the hybrid were uniformly dispersed and improved mechanical properties were attained.[8] Generally, the main reason for such synergistic improvements in nanocomposite systems is still under consideration. According to the current understanding, the factors such as quantum size and columbic charging effects and interfacial interactions related to the ultra fine size and morphologies of the nanofillers form the basis for enhancement. Another belief is that the local and global conformations of polymers within the nanolayers of fillers are different than in the bulk, because the polymer chains are confined in the layers and usually there are no polymer surface interactions in the bulk affecting the local and chain dynamics.[9] To date, there have been many studies dealing with the effects of clay reinforcements on various polymers, e.g., epoxy,[10,11] polystyrene,[12,13] poly(ethylene terephthalate),[14,15] polyurethane,[16,17] nylon-6,[8,18] and nylon-6,6.[19,20]

With its low prices and relatively balanced properties, polypropylene (PP) as matrix, is a good candidate for polymer clay nanocomposites. However, because of its nonpolar nature, it is very difficult to obtain intercalated or exfoliated nanocomposite. The use of a polymeric compatibilizer such as PP-*g*-MA (maleic anhydride grafted PP) enables the formation of intercalated nanocomposite via melt intercalation method.[21,22] Melt rheology data are useful in interpreting the state of dispersion in the melt state and the orientation of clay layers. As reported by Nam et al.,[23] an improved storage modulus was obtained, depending on the degree of intercalation and the

Correspondence to: T. Tinçer (teotin@metu.edu.tr).

TABLE I
Some Properties of As-Received and Powder Serpentine

Property	Specification
Physical appearance	Oily luster, brownish green
Structure	Mainly lizardite, chrysotile
Morphology	platelet
Specific gravity	2.5
Average particle size (μm)	3.3
BET surface area (m^2/g)	61.2

aspect ratio of the dispersed clays. Kawasumi et al.[24] obtained almost complete hybrids with higher storage modulus, when compared to PP, especially between the T_g of PP and 90°C. An increase in storage modulus with the addition of clay particles and even pronounced enhancement in the presence of a PET compatibilizer has been reported by Velasco et al.[25] A study done by Kodgire et al.[26] showed that the mechanical and thermal properties of the PP/PP-*g*-MA/clay system were significantly enhanced; exhibiting a 35% increase in tensile modulus and 10% increase in tensile strength. Depending on the level of dispersion of clay, the thermal degradation temperature increased from 270 to 400°C, as a result of clay incorporation.

PP/serpentine composites with and without silane coupling agent treatment were studied up to 20 wt % filler in the previous study,[27] in which serpentine proved to be very promising filler to reinforce the PP matrix. The layered structure of serpentine enables to obtain intercalated PP/serpentine nanocomposites by the use of its potentiality in separation of layers and following penetration of polymer chains through the expanded layers. Reinforcing ability of serpentine could be further increased with modification of the matrix with PP-*g*-MA and serpentine with quaternary ammonium salt (QAS), leading to PP/serpentine nanocomposites. The current article focuses on the preparation of the nanocomposites through melt intercalation method starting from pristine serpentine, as well as optimization of parameters, i.e., the amounts of reinforcing filler and compatibilizer.

EXPERIMENTAL

Materials

The PP used was HE125M0 25308 grade (melt flow index of 12.0 g/10 min at 230°C/2.16 kg and specific gravity of 0.908), supplied by Borealis AG, Vienna, Austria. Serpentine collected as rocks from Ankara-Beynam region was used as reinforcing clay. As already stated in detail, in our previous work,[27] prior to nanocomposite production, its size was reduced to ~ 3 μm through grinding and ball milling procedures. Some properties of this mineral are tabulated in Table I. PP-*g*-MA compatibilizer with a melt mass flow rate of 5.7 g/10 min at 230°C and specific gravity of 0.89 was provided by Admer® (QF551A grade). The Silane A-1100 (γ-aminopropyl triethoxy silane), early product of Union Carbide (Hahnville, LA), was used as a silane coupling agent (SCA). A QAS of cetyl-trimethyl-ammonium bromide, a product of The British Drug Houses Ltd. (UK), was used as an intercalating agent for serpentine.

Preparation of nanocomposites

The nanocomposites with 2 and 5 wt % serpentine were prepared at PP-*g*-MA to serpentine ratio of 2 : 1 and 3 : 1 by weight. Before QAS treatment, serpentine powders were dispersed in water by stirring overnight. The pH of the solutions was maintained at 3 with concentrated HCl. Then, QAS was added to the solution (serpentine/QAS = 10/3 by weight) and the mixture was stirred continuously at 70°C for 24 h. An additional mixing of 5 h, without heating, was followed by vacuum filtering. SCA treatment was applied to all compositions at a 1 : 46 weight ratio of SCA to serpentine. The coupling agent was dissolved in diethyl ether and the filler was added, with vigorous mixing. To remove the diethyl ether and get rid of any moisture, the powders were dried overnight at 100°C. Table II shows the different compositions under study.

A two-step extrusion process was used to prepare the samples. In the first step, PP-*g*-MA and serpentine were compounded in accordance with the desired ratio. Then, the masterbatches were dry-mixed with PP, fed into the main feeder and extruded. Melt blending was carried out, using the Thermoprism TSE 16 TC (Newington, NH), corotating and intermeshing twin screw extruder (D = 16 mm, L = 384 mm). While the barrel temperatures were fixed at 220°C from hopper to die, the feed rate and the screw speed were 20 g/min and 190 rpm, respectively. Following to pelletizing and drying at 80°C, extruded samples were molded by

TABLE II
Designations of all Compositions Studied

Sample	PP	Serpentine	PP-*g*-MA	QAS treatment[a]
PP	100	–	–	–
PP-2,4	94	2	4	–
PP-2,4Q	94	2	4	x
PP-5,10	85	5	10	–
PP-5,10Q	85	5	10	x
PP-2,6	92	2	6	–
PP-2,6Q	92	2	6	x
PP-5,15	80	5	15	–
PP-5,15Q	80	5	15	x

Where x indicates QAS treatment in far right column.

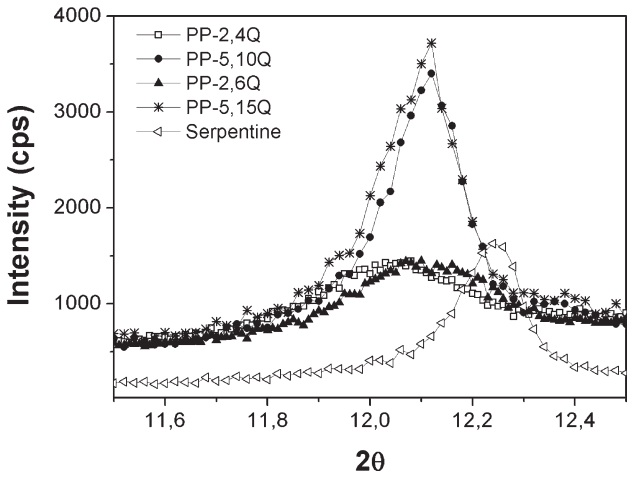

Figure 1 XRD patterns of serpentine and PP/serpentine nanocomposites.

Microinjector, Daca Instruments, laboratory scale type injection molding machine at a barrel temperature of 220°C.

Characterization methods

The nanocomposites were analyzed by D8 Advance Bruker X-ray diffractometer by employing CuKα radiation with $\lambda = 1.54$ Å, 40 Kv, and 40 mA source. The diffraction pattern was recorded between 5° and 30° 2θ range and at a scanning rate of 1°/min and steps of 0.01°.

To investigate the nanometer scale distribution and micro morphology of filler layers, transmission electron microscopy (TEM) analysis was carried out using a Jeol JEM-2000FX STEM on the specimens cut from the middle portion of injection molded samples. LKB CryoNova Cryoultramicrotome was used to obtain ultra thin sections of nearly 100 nm thick. Then they were placed on formvar carbon coated copper grids (300 mesh) and analyzed at an accelerating voltage of 200 kV.

Differential scanning calorimetry (DSC) analysis was performed using a Dupont Thermal Analyst 2000 DSC 910 S between 20°C and 200°C, under N_2 atmosphere with a heating rate of 10 °C/min. The percentage crystallinity of the nanocomposites was calculated according to the equation:

$$\chi = \frac{\Delta H}{\Delta H_{100}}\%,$$

where χ is the percentage crystallinity, ΔH is the enthalpy heat of fusion of composite and ΔH_{100} is the enthalpy heat of fusion for an ideally 100% crystalline PP (209 J/g).[28]

Dynamic mechanical analysis (DMA) of the injection molded specimens was studied using the Perkin–Elmer Pyris Diamond DMA in the tensile mode, according to ASTM D4092, from −60 to 70°C. The samples were tested with an oscillating amplitude of 5 μm, a frequency of 10 Hz, and a heating rate of 5 °C/min.

Tensile properties were determined on an Instron Tensile Testing Machine, TM1102, at a drawing rate and gauge length of 50 mm/min and 75 mm, respectively, (ASTM D638). In all mechanical tests, at least seven specimens were tested for each composition.

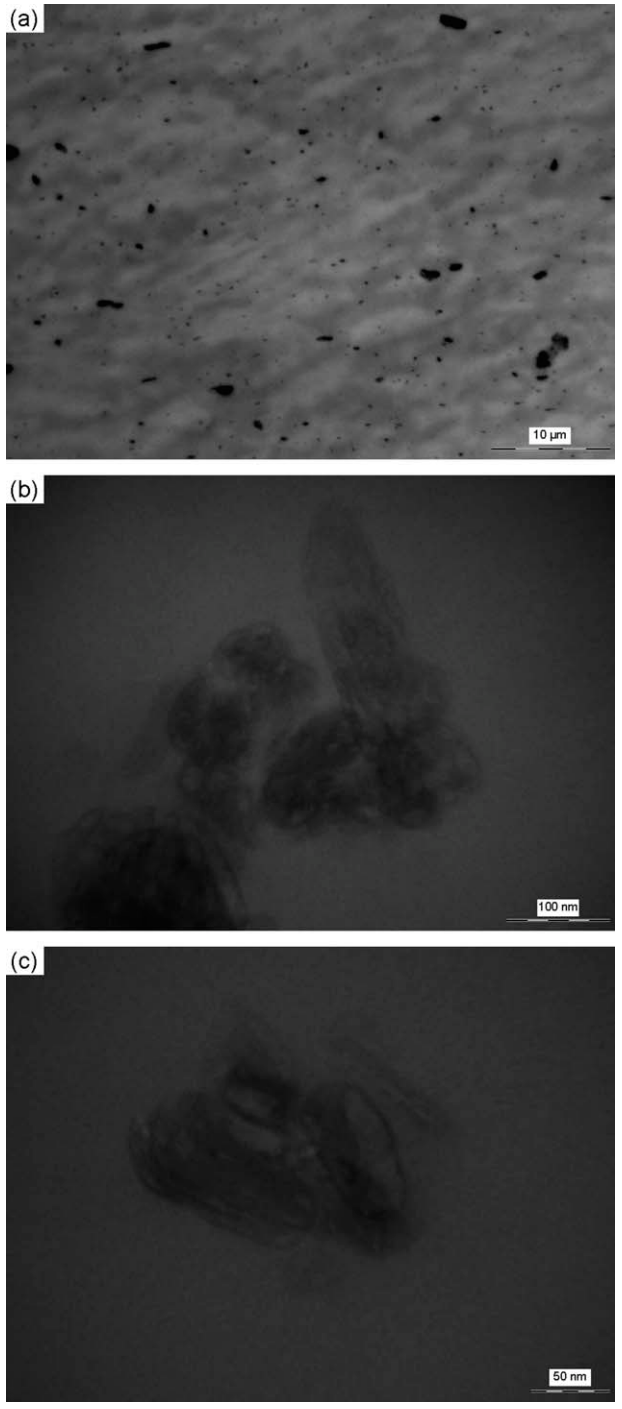

Figure 2 TEM micrographs of (a) PP-2,4Q, (b) PP-5,10Q, and (c) PP-2,6Q.

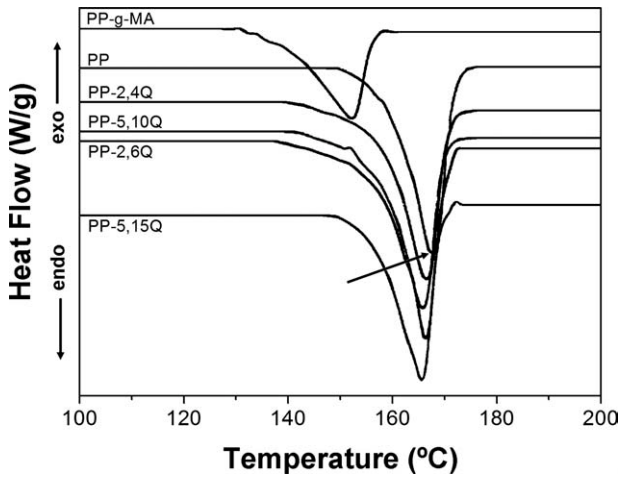

Figure 3 DSC thermograms of PP-*g*-MA, PP and PP/serpentine nanocomposites. (The arrow shows the melting temperature of PP).

RESULTS AND DISCUSSION

Structural analysis

The structure of nanocomposites was studied using the X-ray diffraction (XRD) and the transmission electron microscopy (TEM) techniques. Figure 1 illustrates the XRD patterns for serpentine and PP/serpentine nanocomposites. Bragg's law was used to calculate the *d*-spacing of specimens from the diffraction data. It is seen from the figure that serpentine shows an intense peak at 2θ of 12.24°, which corresponds to a *d*-spacing of 7.22 Å. For the nanocomposites, the shifting of diffraction peaks to higher *d*-spacing by extending the intergallery spacing of the silicate mineral is an indication of intercalation of polymer chains through the clay layers. The serpentine peak at 12.24° shifted to lower angles for all nanocomposites. Although the shift in samples is nearly the same, PP-2,4Q showed the maximum decrease in 2θ by 0.22° (or an increase of *d*-spacing to 7.35 Å) compared to serpentine. This observation can be correlated to the intercalation of PP chains into the serpentine layers. The resultant nanocomposites can be said to be slightly intercalated, since the amount of shift is very small. The initial interlayer spacing plays an important role such that larger separation leads to an easy intercalation/exfoliation of clay platelets. Due to the decreased interactions between the clay layers, polymer chains may diffuse into the clay galleries without difficulty. Considering the fact that serpentine is a 1 : 1 layered silicate with a lower *d*-spacing than frequently used 2 : 1 structured clays, it is not easy to obtain intercalated/exfoliated nanocomposites. Yet, hydrophobic PP has low affinity for hydrophilic serpentine layers.

Figure 2 displays the TEM micrographs for PP-2,4Q, PP-5,10Q, and PP-2,6Q compositions at different magnifications. The light colored area represents the PP matrix and the darker regions correspond to serpentine layers. Although, for all the samples analyzed, homogeneous distribution was observed, small amount of aggregation is evident from low magnification TEM images, as demonstrated for PP-2,4Q. At high magnifications, stacked parts of the filler are seen due to the clustering and aggregation of the layers. Since the shift of *d*-spacing is low for the nanocomposites, separate layers were not detected.

Differential scanning calorimetry

DSC was used to determine the melting temperatures and the percentage crystallinity of nanocomposites. The thermograms are illustrated in Figure 3. Neat PP exhibited a single and sharp endotherm at 167.0°C, that belongs to the α-phase, which is the most common crystal form of isotactic-PP. PP-*g*-MA demonstrated a broad melting range between onset T_m (melting temperature) of 134.5°C and the peak at 152.8°C, and low melting enthalpy with respect to PP. Although maleated polymers usually exhibit a shoulder on their melting endotherms, this is not very pronounced for the PP-*g*-MA used in this study. The only thermogram that shows a shoulder before the melting point of PP is in the sample PP-5,10Q. The shape of its melting endotherm reveals that PP-*g*-MA does not have uniform crystal formation. This can be expected since the presence of graft functional groups may affect negatively the crystalline sizes of PP. The melting points of the nanocomposites demonstrated a decrease when compared to that of neat PP. PP-2,4Q and PP-2,6Q showed melting at about the same point; i.e., 166.4°C and 166.3°C, respectively. For the samples with high content of compatibilizer, the reduction is more evident,

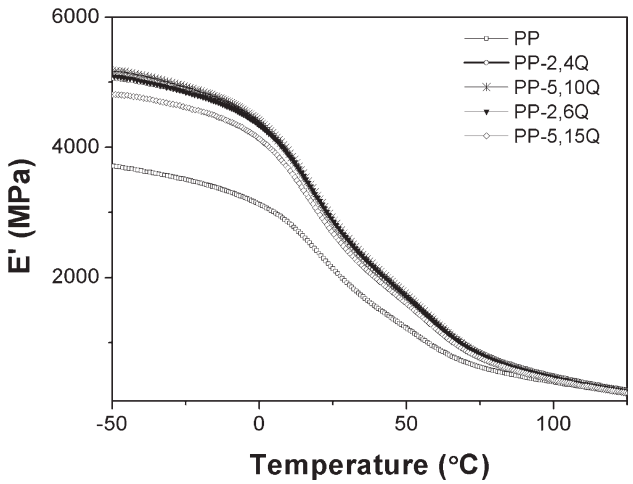

Figure 4 The storage moduli of PP and its nanocomposites as a function of temperature.

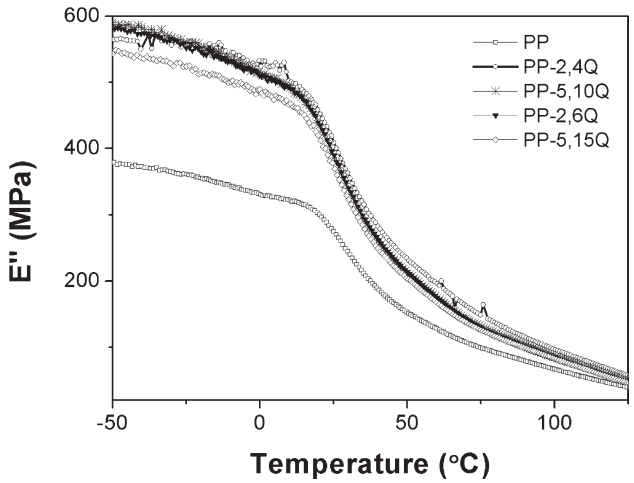

Figure 5 The loss moduli of PP and its nanocomposites as a function of temperature.

and the decrease is around 2°C. The crystallites formed due to the graft functional groups have less stability than neat PP. It is expected that the reduction in melting temperatures would be higher in the absence of serpentine. It is apparent that the filler, somewhat, compensated the reduction in melting temperatures. The reason might be that enhanced filler–matrix interaction led to more stabilized structure in the presence of filler. The change in percentage crystallinity of the nanocomposites when compared to PP was calculated to observe the effect of serpentine on the crystallization behavior. While the percentage crystallinity of neat PP was 29.8, the nanocomposites PP-2,4Q, PP-5,10Q, PP-2,6Q, and PP-5,15Q exhibited percentage crystallinity values of 31.3, 33.9, 32.7, and 33.5, respectively. The increase in percentage crystallinity of composites can be explained by the role of filler as a nucleating agent, leading to heterogeneous nucleation and increase in the percentage crystallinity.

Dynamic mechanical analysis

DMA experiment was conducted to study the performance of the nanocomposites under dynamic loading and variable temperature. The addition of rigid, inorganic filler inevitably affects the bulk properties, especially, the modulus. The results for storage and loss moduli *versus* temperature are given in Figures 4 and 5. As seen from both graphs, the modulus decreases with temperature due to the increased polymer segmental motion at high temperatures. The representative storage modulus (and also relative storage modulus) values are listed in Table III at temperatures −40°C, 0°C, 40°C, 80°C, and 120°C. The relative storage modulus values at temperatures from −40 to 40°C changed between 1.3 and 1.4 for all samples. Although, there is a slight decrease at high temperatures, storage moduli of nanocomposite samples are higher than that of neat PP. It should be noted that, the same trend is seen for loss moduli as in storage moduli; higher loss modulus was observed in the case of serpentine-filled PP when compared to the neat matrix. While PP-2,4Q showed the highest storage moduli, PP-5,15Q exhibited the lowest moduli values in the temperature range studied. This behavior is in close resemblance to the tensile Young's modulus as well as other tensile properties of PP-5,15Q. Therefore, it is apparent that there are certain compositions of PP-*g*-MA/serpentine ratio that lead to better properties. Additionally, the rubbery plateau region gives information about the crystallinity of the material.[29] The neat PP has lower storage and loss moduli in comparison with the serpentine-filled samples, an indication of low crystallinity than the nanocomposites. A marginal upward shift of the plateau for the nanocomposites corresponds to higher crystallinity, which is in agreement with DSC results.

Mechanical properties

Tensile properties of the compositions without QAS treatment (neat compositions) were also reported in this part. Previously noted in the structural analysis part was the fact that QAS treatment led to slightly intercalated PP/serpentine nanocomposites. The emphasis on mechanical properties illustrates the effect of QAS treatment more clearly.

The Young's modulus, measured by static methods, strongly corroborates what was observed in dynamic measurements. The addition of serpentine, even in the presence of soft and weak material PP-*g*-MA,

TABLE III
Storage Modulus (E') of PP and its Nanocomposites at Various Temperatures

Sample	−40°C	0°C	40°C	80°C	120°C
PP	3.64	3.12	1.52	0.56	0.25
PP-2,4Q	5.00 (1.37)	4.36 (1.40)	2.07 (1.36)	0.75 (1.34)	0.31 (1.24)
PP-5,10Q	5.10 (1.40)	4.38 (1.40)	2.11 (1.39)	0.70 (1.25)	0.27 (1.08)
PP-2,6Q	5.02 (1.38)	4.35 (1.39)	2.10 (1.38)	0.72 (1.29)	0.28 (1.12)
PP-5,15Q	4.76 (1.31)	4.13 (1.32)	1.97 (1.30)	0.67 (1.20)	0.26 (1.04)

Relative storage modulus (E'_{NC}/E'_{PP}) values are shown in parentheses.

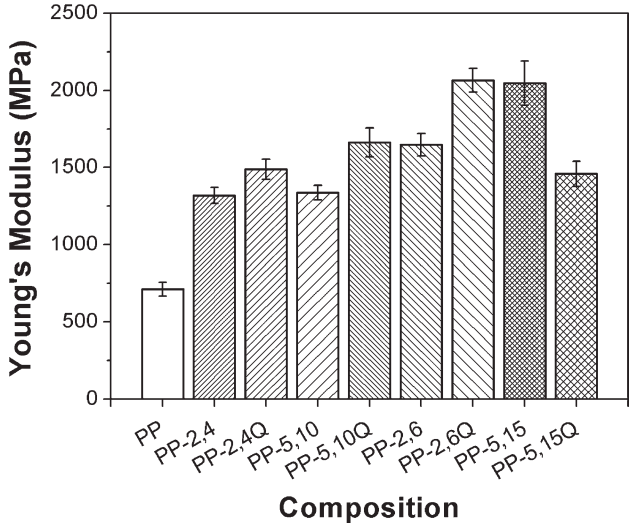

Figure 6 Young's Modulus of PP and its nanocomposites (with their neat compositions) *versus* composition.

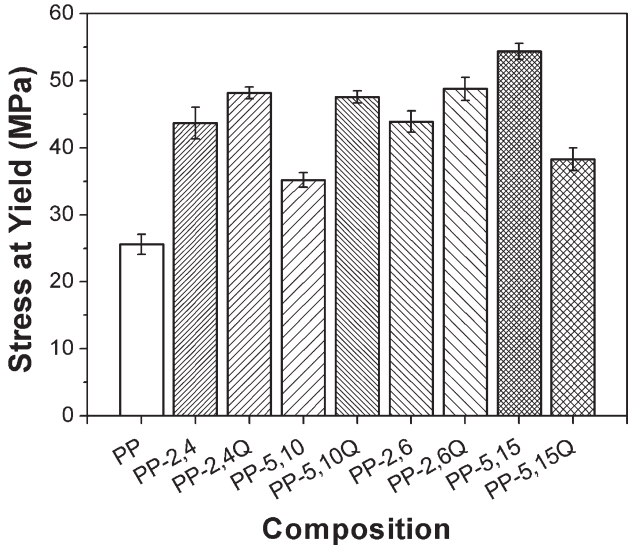

Figure 8 Yield stress of PP and its nanocomposites (with their neat compositions) *versus* composition.

improves the modulus, to varying extents. Young's modulus values increased with respect to the neat compositions, as exemplified in Figure 6. PP-5,15Q showed the lowest modulus among all nanocomposites as it did in storage and loss moduli. The modulus of PP-2,4Q is 109.6% and PP-5,10Q is 134% greater than that of unfilled PP. The maximum improvement was in PP-2,6Q nanocomposite, corresponding to 2065 MPa, i.e., 190.8% and 25.3% increase when compared to the neat PP and PP-2,6, respectively. This increase can be attributed, simply, to the restriction of mobility of the polymer chains because of the constraints imposed on them by the filler layers, hence leading to high modulus values. Previous study[27] also illustrated the fact that SCA treatment is also effective between the interface of serpentine and PP matrix, resulting in high modulus values.

The results of other tensile tests are given in Figures 7–9. The tensile strength of composites showed a similar variation with tensile modulus; filled PP samples have significantly higher ultimate strength when compared to neat resin. For nanocomposites (both PP-*g*-MA and QAS treated), the highest value was attained with sample PP-5,10Q (47.6 MPa), that is, the tensile strength increased by 88.1% and 34.1% when compared to unfilled PP and PP-5,10, respectively. The explanation is the same as in the Young's modulus, i.e., improved interfacial bonding between serpentine and PP resulted in better tensile strength values. While PP-2,4 and PP-2,6 compositions

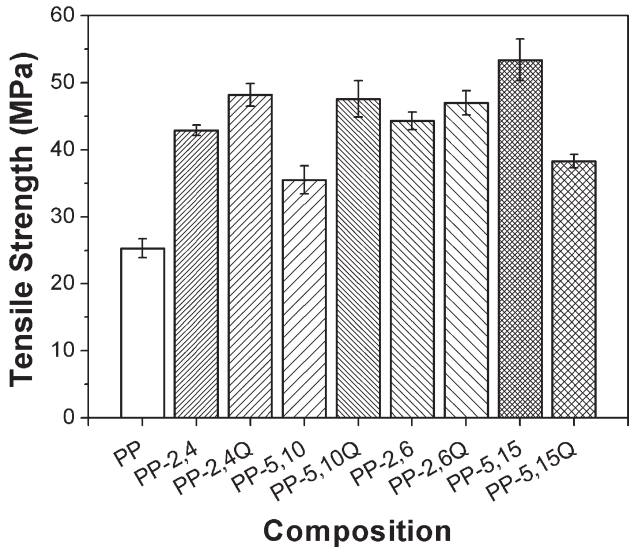

Figure 7 Tensile strength of PP and its nanocomposites (with their neat compositions) *versus* composition.

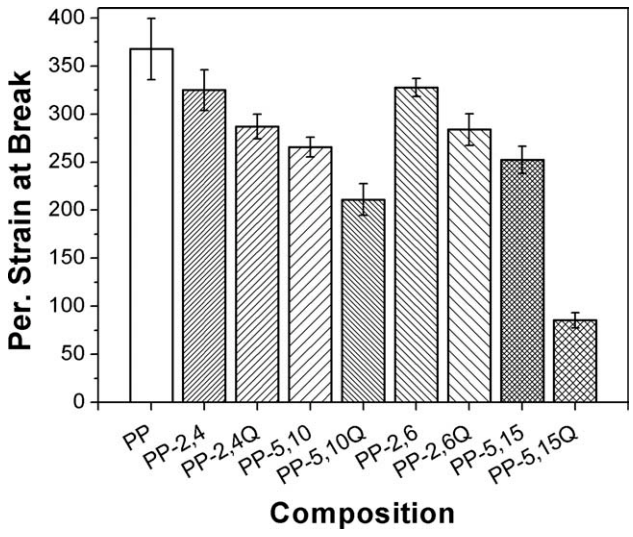

Figure 9 Percentage strain at break of PP and its nanocomposites (with their neat compositions) *versus* composition.

exhibited nearly the same yield stress (~ 44 MPa), PP-5,10 had a lower value (35 MPa), as seen in Figure 8. This decrease can be correlated to the increase in filler content. As the concentration of filler increases, the amount of total interphase area between matrix and the filler also increases which may lead to higher stress concentration and lower yield stress values. However, the maximum yield stress was attained at 54.4 MPa for PP-5,15 composition at the same filler content. The reason might be attributed to the high PP-*g*-MA content of PP-5,15 indicating that compatibilizer may compensate the filler effect for this composition. Apart from PP-5,15 and PP-5,15Q, QAS treatment increased the yield stress with respect to neat compositions, which reached a maximum at 48.8 MPa for PP-2,6Q. The elongation-at-break of compositions is shown in Figure 9. Expectedly, neat PP has the highest value which is 367.6. PP-2,4 and PP-2,6 compositions exhibited elongations of 324.9 and 327.7, respectively, with a slight reduction when compared to the neat matrix. Upon the increase of serpentine content, resistance to plastic deformation increased, leading to a further decrease for PP-5,10 and PP-5,15. However, even in this case, the reductions are not very obvious: as it is to be expected due to the presence of rigid filler. It is apparent that, PP/serpentine nanocomposites are plastically deformable with very high tensile modulus and ultimate tensile strength.

CONCLUSIONS

This article investigated the dispersion of serpentine filler in the PP matrix and the properties of the resultant nanocomposites. The intercalation of serpentine layers was achieved throughout the PP matrix for the first time. Although the intercalation is limited, the PP/serpentine nanocomposites demonstrated superior properties when compared to the neat PP. The nanocomposite with 2 wt % serpentine and 6 wt % PP-*g*-MA (PP-2,6Q) showed a Young's modulus value of 2065 MPa, a substantial increase when compared to that of neat PP, i.e., 710 MPa. In the previous study, at the same filler content, silane treated PP/serpentine composite exhibited a Young's modulus of 1218 MPa. This comparison clearly shows that, serpentine is further effective to reinforce PP in its nanocomposites, making it as a powerful nanofiller for the PP matrix.

References

1. Vaia, R. A.; Jandt, K. D.; Kramer, E. J.; Giannelis, E. P. Chem Mater 1996, 8, 2628.
2. Hambir, S.; Bulakh, N.; Jog, J. P. Polym Eng Sci 2002, 42, 1800.
3. Liu, J.; Boo, W. J.; Clearfield, A.; Sue, H. J Mater Manuf Process 2006, 20, 143.
4. Geckeler, K. E.; Rosenberg, E. Functional Nanomaterials; American Scientific Publishers: California, 2006.
5. Kozak, M.; Domka, L. J Phys Chem Solids 2004, 65, 441.
6. Baldassari, S.; Komerneni, S.; Mariani, E.; Villa, C. Appl Clay Sci 2006, 31, 134.
7. Okamoto, M. Polymer/Layered Silicate Nanocomposites; Rapra Techonology Limited: Boston, 2003; Vol. 14.
8. Kojima., Y.; Usuki, A.; Kawasumi, M.; Okada, A.; Kurauchi, T.; Kamigaito, O. J Polym Sci Pol Chem 1993, 31, 983.
9. Yuan, M.; Misra, R. D. K. Polymer 2006, 47, 4421.
10. Lan, T.; Pinnavaia, T. J Chem Mater 1994, 6, 2216.
11. Ryu, J. G.; Park, G. R.; Lyu, S. G.; Rhew, J. H.; Sur, G. S. Polym-Korea 1998, 22, 328.
12. Fu, X.; Qutubuddin, S. Mater Lett 2000, 42, 12.
13. Moet, A. S.; Akelah, A. Mater Lett 1993, 18, 97.
14. Ke, Y. C.; Long, C. F.; Qi, Z. N. J Appl Polym Sci 1999, 71, 1139.
15. Ou, C. F.; Ho, M. T.; Lin, J. R. J Appl Polym Sci 2004, 91, 140.
16. Chen, T. K.; Tien, Y. I.; Wei, K. H. Polymer 2000, 41, 1345.
17. Wang, Z.; Pinnavaia, T. J Chem Mater 1998, 10, 3769.
18. Usuki, A.; Koiwai, A.; Kojima, Y.; Kawasumi, M.; Okada, A.; Kurauchi, T.; Kamigaito, O. J Appl Polym Sci 1995, 55, 119.
19. Mert, M.; Yilmazer, U. J Appl Polym Sci 2010, 118, 209.
20. Mert, M.; Yilmazer, U. J Appl Polym Sci 2008, 108, 3890.
21. Koo, C. M.; Kim, J. H.; Wang, K. H; Chung, I. J. J Polym Sci Part B: Polym Phys 2005, 43, 158.
22. Hambir, S.; Bulakh, N.; Kodgire, P.; Kalgaonkar, R.; Jog, J. P. J Polym Sci Part B: Polym Phys 2001, 39, 446.
23. Nam, P. H.; Maiti, P.; Okamoto, M.; Kotaka, T.; Hasegawa, N.; Usiki, A. Polymer 2001, 42, 9633.
24. Kawasumi, M.; Hasegawa, N.; Kato, M.; Usiki, A.; Okada, A. Macromolecules 1997, 30, 6333.
25. Velasco, J. I.; Ardanuy, M.; Realinho, V.; Antunes, M.; Fernandez, A. I.; Gonzalez-Pena, J. I.; Rodriguez-Perez, M. A.; de Saja, J. A. J Appl Polym Sci 2006, 102, 1213.
26. Kodgire, P.; Kalgaonkar, R.; Hambir, S.; Bulakh, N.; Jog, J. P. J Appl Polym Sci 2001, 81, 1786.
27. Tan, S.; Tincer, T. J Appl Polym Sci 2011, 121, 846.
28. Brandrup, J.; Immergut, E. H. Polymer Handbook; Wiley-Interscience Publication: New York, 1989.
29. Menard, K. P. Dynamic Mechanical Analysis: A Practical Introduction; CRC Press: Boca Raton, 1999.